

# Internal Structure of Massive Terrestrial Planets

Diana Valencia<sup>a,1</sup>, Richard J O'Connell<sup>a</sup> and Dimitar Sasselov<sup>b</sup>

<sup>a</sup> Earth and Planetary Sciences, Harvard University, Cambridge, Massachusetts, 02138

<sup>b</sup> Harvard-Smithsonian Center for Astrophysics, Department of Astronomy, Harvard University, Cambridge, Massachusetts, 02138

<sup>1</sup>Corresponding Author E-mail address: valencia@mail.geophysics.harvard.edu

## ABSTRACT

Planetary formation models predict the existence of massive terrestrial planets and experiments are now being designed that should succeed in discovering them and measuring their masses and radii. We calculate internal structures of planets with one to ten times the mass of the Earth (Super-Earths) in order to obtain scaling laws for total radius, mantle thickness, core size and average density as a function of mass. We explore different compositions and obtain a scaling law of  $R \propto M^{0.267-0.272}$  for Super-Earths. We also study a second family of planets, Super-Mercuries with masses ranging from one mercury-mass to ten mercury-masses with similar composition to the Earth's but larger core mass fraction. We explore the effect of surface temperature and core mass fraction on the scaling laws for these planets. The scaling law obtained for the Super-Mercuries is  $R \propto M^{\sim 0.3}$ .

**Key words:** Extrasolar Planets, Interiors, Terrestrial Planets

# 1 Introduction

In the last decade, astronomers have indirectly detected more than 160 planets orbiting stars other than our Sun. The two methods used most extensively are 1) the radial velocity method that uses the Doppler shift in the parent star's motion caused by the orbiting planet and 2) the method of transits that uses the periodic drop in brightness of the star as the planet eclipses it in its motion around it. There is very little known about these new planets, since no direct observations have been made yet, however in at least one case the transit observations led to the detection of the planet's atmosphere (Charbonneau et al. 2002, Vidal-Madjar et al. 2003). Also, by combining the two methods one can determine both the planet's mass and radius, yielding some insight into their interior structure. For seven extrasolar planets in the mass range of  $0.5 - 1.5 M_{Jup}$  the estimated mean bulk densities range from  $0.4 - 1.3 g cm^{-3}$  (Konacki et al. 2005). These imply gas giant planet structure similar to that of Jupiter and Saturn.

Up to this point all extrasolar planets discovered have been gas giants. A large fraction of them are in very tight orbits (with periods of a few days) making their surface temperature very hot (Hot Jupiters). Only in the past year have discoveries reached masses as small as those of Neptune and Uranus. Certainly all search methods are biased to detect the largest and most massive planets, but the frontier is being quickly pushed down using both higher precision as well as a larger and diverse sample of stars. Space missions under development, such as Kepler (Borucki et al. 2003) and COROT (Baglin et al. 2002), are fully capable (and expected) to discover many massive terrestrial planets (Super-Earths); the Kepler mission expects to discover almost one thousand Super-Earths. Such expectations are based in part on theoretical work that shows no evidence precluding planet formation in the  $1 - 10 M_{\oplus}$  mass range (e.g. Ida and Lin 2004), even in planetary systems with Hot Jupiters (Lunine et al. 2004). Therefore, we believe it is timely to compute models of the internal structure of Super-Earths and study the possible mass-radius relations, especially because we have found no such previous work in the literature.

Though, far from complete, our understanding of the Earth is the most comprehensive that we have of any planet and should be the starting point to study massive terrestrial planets. In this paper we have scaled Earth to more massive planets as the first step into understanding how other terrestrial planets might have accreted and evolved. We address the likelihood of existence of these planets in section two. In section three we describe the method we use to obtain the density distribution, pressure and temperature profiles of ten planets spanning from one earth-mass to ten earth-masses with same chemical and mineral composition as the Earth, which from here on will be called Super-Earths. Scaling laws are derived for the total radius, mantle thickness, core radius and average mantle density as the total mass of an Earth-like planet increases.

It will become clear in section three that an a-priori assumption on the ratio of Fe/Mg

needs to be made to account for the amount of mass of the planet in the core. Therefore, in section three we consider another family of planets with different Fe/Mg ratio, corresponding to the ratio believed for Mercury, and with masses ranging from one mercury-mass to ten mercury-masses (Super-Mercuries), and we investigate the effect of surface temperature on the scaling laws.

## 2 On the Formation of Super-Earths

Given the obvious lack of terrestrial planets of mass between  $1 - 10 M_{\oplus}$  in our own Solar System, it is appropriate to investigate if such planets are unlikely to form. As we shall see all indications are that they will. First, in reconstructing the minimum-mass solar nebula (the proto-planetary disk that gave rise to the Solar System planets), as well as our current knowledge of what are typical proto-planetary disks (Hayashi 1981, Wetherill 1990, Beckwith and Sargent 1996, Wyatt et al. 2003), we find plenty of solid material to accumulate planets larger than the Earth. Most generally (including orbit migration), what limits the masses of rocky planets in the inner parts of a disk (few AU [Astronomical Unit=  $a_{\oplus}$ ] from the star) is the available amount of solid material (Ida and Lin 2004):

$$M \simeq 1.2\eta_{ice}f\left(\frac{a}{1 AU}\right)^{1/2} M_{\oplus}$$

where  $f$  is a scaling parameter for the total disk mass (typical values are in the 0.1–30 range),  $\eta_{ice}$  is a step function (jumps from 1 to  $\sim 4$ ) describing the increase in density of solid particles as ice condenses outside the 'snow line' at an orbital distance,  $a$ , of a few AU.

Second, as a planet embryo of mass  $M$  grows above about an Earth mass, it begins to accrete gas from the disk. Such accretion could quickly turn into a runaway process that would lead to the formation of a gas giant planet like Jupiter (Mizuno 1980, Stevenson 1982, Bodenheimer and Pollack 1986). The value of the critical mass,  $M_{crit}$ , for which such runaway growth can occur would thus determine whether Super-Earths are likely to exist at all.

Precise determination of  $M_{crit}$  would require 3-dimensional radiation hydrodynamics models. Current simpler numerical models (Ikoma et al. 2000) find a robust dependence on the rate of accretion,  $\dot{M}$ , and the opacity,  $\kappa$ , of the disk gas:

$$M_{crit} \simeq 10\left(\frac{\dot{M}}{10^{-6}M_{\oplus}yr^{-1}}\right)^q\left(\frac{\kappa}{1cm^2g^{-1}}\right)^s M_{\oplus},$$

where  $q$  and  $s$  lie between 0.2 and 0.3. One might expect that planets grow so rapidly from  $\sim 10$  to more than  $100M_{\oplus}$  that they would rarely be found with a final mass in the intermediate range ( $10 - 100 M_{\oplus}$ ), as shown by the detailed calculations of Ida & Lin (2004). These same calculations predict a large number of Super-Earths in the inner parts of the disk. It is important to note that a certain fraction of the Super-Earths will have a substantial volatile content (primarily water); while dry terrestrial planets are most common in the inner disk,

the expected fraction of 'ocean planets' is poorly known (Raymond et al. 2004).

We hence conclude that the common existence of Super-Earths ( $1 - 10 M_{\oplus}$ ) is a reasonable expectation of the current theory of planet formation.

### 3 Earth and Super-Earths

#### 3.1 Method

In a radially symmetric planet that is chemically and mineralogically homogeneous the equations describing the density  $\rho$  (Adam-Williamson equation), gravity  $g$ , mass  $m$  and pressure  $P$  derivatives are:

$$\frac{d\rho}{dr} = -\frac{\rho(r)g(r)}{\phi(r)} \quad (1)$$

$$\frac{dg}{dr} = 4\pi G\rho(r) - \frac{2Gm(r)}{r^3} \quad (2)$$

$$\frac{dm}{dr} = 4\pi r^2 \rho(r) \quad (3)$$

$$\frac{dP}{dr} = -\rho(r)g(r) \quad (4)$$

where  $\phi(r) = \frac{K_S(r)}{\rho(r)}$  is the seismic parameter that can be calculated from equations of state,  $K_S$  is the adiabatic bulk modulus,  $G$  is the gravitational constant and  $r$  is the distance from the center of the planet.

The equation of state (EOS) we choose is the third order Birch-Murnaghan equation of state with a Debye thermal correction. This EOS results from the expression of the Helmholtz free energy as a power series expansion of finite strain and the thermal correction accounts for lattice vibrations with a cut-off frequency corresponding to the Debye frequency. This EOS has been shown to be adequate for our purposes (Birch 1952, Poirier 2000a) and its expression is the following

$$K_T(\rho, T) = K_T(\rho, 300) + \Delta K_{th}(\rho, T) \quad (5)$$

$$K_T(\rho, 300) = \frac{K_{0,300}}{2} \left\{ (7x^{7/3} - 5x^{5/3}) \left[ 1 + \frac{3}{4} (K'_{0,300} - 4) (x^{2/3} - 1) \right] + \frac{3}{2} (x^{9/3} - x^{7/3}) (K'_{0,300} - 4) \right\}$$

$$\Delta K_{th} = 3nR\gamma\rho (f(T) - f(T_0))$$

$$f(T) = (1 - q - 3\gamma) \frac{T^4}{\theta^3} \int_0^{\frac{\theta}{T}} \frac{\xi^3 d\xi}{\exp \xi - 1} + 3\theta\gamma \frac{1}{\exp(\theta/T) - 1}$$

$$K_S = K_T \{1 + \alpha\gamma T\}$$

where  $K_{0,300}$  and  $K'_{0,300}$  are the isothermal bulk modulus and its first derivative at zero pressure and  $T_0 = 300\text{K}$ ;  $K_T$  and  $K_S$  are the isothermal and adiabatic bulk modulus at any given radius;  $x(r) = \frac{\rho(r)}{\rho_0}$  is the ratio of density to the uncompressed density;  $\alpha$  is the coefficient of thermal expansion;  $R$  is the universal gas constant;  $n$  is the number of atoms in the unit cell;  $\theta$  is the Debye temperature and  $\gamma$  is the Gruneisen parameter taken to vary with depth as  $\theta = \theta_0 \exp\left(\frac{\gamma_0 - \gamma}{q}\right)$  and  $\gamma = \gamma_0 \left(\frac{\rho_0}{\rho(r)}\right)^q$ . This EOS does not include a contribution from electronic pressure in metals known to have a 8% contribution to pressure at 350 GPa compared to a 22% contribution from thermal pressure (Stixrude and Wasserman 1997). Our results are not affected by this term and will be discussed in section 3.

The system of PDE's described in Eq. 1 to 4 in conjunction with Eq. 5 is integrated numerically from the surface using a fourth order Runge-Kutta algorithm with initial conditions of a given surface density, zero surface pressure, total mass  $M$ , and corresponding surface gravity  $g_s = GM/R^2$ , where  $R$  is the total radius. The algorithm searches for an appropriate total radius corresponding to a fixed total mass  $M$  and composition included in the values for  $\rho_0, K_{0,300}, K'_{0,300}, \gamma_0, q$  and  $\theta_0$  in the EOS and stops when it finds a total radius that yields no excess mass in the last inner shell of the integration.

Because the Earth is not homogeneous in composition we need to include mixtures between different mineral phases in the different regions of the Earth. There are two approaches that can be implemented: to use the thermodynamic values at some reference state ( $T=300$  and atmospheric pressure) as an equivalent of the mix of the mineral components for each region (upper mantle, transition zone, lower mantle, outer core, inner core), or mix the different mineral phases at each radius of the integration by performing a weighted by mol linear interpolation of the thermodynamic parameters (density, bulk modulus and Gruneisen parameter).

Since the EOS data applies to a particular material, the latter approach is more exact and we have used it in the mantle. Due to the lack of extensive and complete thermodynamic data for iron and iron with lighter elements at relevant pressures and temperatures, we use the first approach for the core. The mineral phases that are considered in the mantle are olivine and high pressure forms of olivine. For the core we used Fe with 8% by weight Si, extreme end members FeO and Fe, and Fe plus some alloy equivalent that best fits the density and bulk modulus data from the PREM model (Dziewonski and Anderson 1981).

In order to include the phase changes that are known to exist in the Earth and are expected to be present in the Super-Earths the temperature profile needs to be calculated. We

use simple boundary layer convection models used to describe mantle convection on Earth (Turcotte and Schubert 2002) to obtain the regions where conduction is present (surface and core-mantle boundary layers) and where convection is present (bulk mantle and core). We assume that the surface boundary layer is mobile, as is the case for Earth. A stagnant lid treatment would yield differences in the sizes of the boundary layers. These differences have an effect on the exact structure of the planet but not on the exponent of the scaling laws we derive in this study.

The temperature gradient through the boundary layers at the surface and core-mantle boundary (CMB) is

$$\frac{dT}{dr} = -\frac{q_{planet}}{k} \quad (6)$$

where  $q_{planet}$  is the heat flux at the surface ( $q_s$ ) or at CMB ( $q_{cmb}$ ) and  $k$  is the thermal conductivity. The mantle is known to be convecting and in this study is taken to be convecting as a single layer. The core is also known to be in a very vigorous convecting regime in order to sustain the Earth's dynamo (Fearn 1998). The convective temperature profiles in the mantle and the core are described by the adiabatic gradient

$$\frac{dT(r)}{dr} = \frac{\rho(r)g(r)T(r)}{K_S(r)}\gamma(r) \quad (7)$$

which holds in the convecting region. At the upper and lower boundaries, heat is transported by conduction through a boundary layer of thickness  $\delta$ . The Rayleigh number governing convection may be expressed in terms of the surface heat flux  $q_s$

$$Ra = \frac{\rho g \alpha q_s / k}{\kappa \eta} D^4 \quad (8)$$

where  $\rho$  is the average upper mantle density,  $\alpha$  is the thermal expansivity,  $\kappa$  is the thermal diffusivity and  $\eta$  is the viscosity. Considering that the dimensionless heat transport should be a function of the Rayleigh number and that the thickness of the boundary layer should not depend on the thickness of the mantle for a vigorously convecting incompressible system (O'Connell and Hager 1980), the expression for the thickness of the surface boundary layer is

$$\delta = a \frac{D}{2} \left( \frac{Ra}{Ra_c} \right)^{-1/4} \quad (9)$$

where  $a$  is a coefficient of order unity. Boundary layer models give the same result (Turcotte and Schubert 2002). We have included the dependency of viscosity on temperature with the relationship  $\eta(T) = \eta_0 \left( \frac{T}{T_0} \right)^{-n}$  with  $n = 30$  proposed by (Davies 1980) to be adequate for the Earth. Parameters in Eq.8 are those for the upper mantle consistent with a boundary layer model in which convection is governed by the stability of the boundary layer.

The heat driving convection in the Earth is a combination of heat produced from within

by radioactive sources and from cooling of the Earth, including heat conducted from the core into the mantle at the CMB. The exact contributions are not well known, thus the thickness of the boundary layer at CMB and the heat conducted down the adiabat in the core are uncertain (Labrosse et al. 2001). In this study the value chosen ad-hoc to describe the conductive region in the mantle at CMB is half the thickness of the surface boundary layer. For planets that reach very high pressures, compressibility effects will become important, and hence, this simple parametric approach will fall short from a true description. In addition, this model assumes that the rheology is relatively uniform, which may not be the case at very high pressures. Nevertheless, it is the first and most simple analytic step to take. Figure 1 shows a schematic diagram of the temperature profile in the Earth’s mantle.

[Figure 1]

The first stage of the numerical modeling includes a planet with only a core and a mantle (ie. no phase transitions). The core mass fraction (CMF) of the Earth is specified a priori as 32.59% (Stacey 1992b) reflecting the Fe/Mg ratio. The EOS in this stage has no thermal corrections since no temperature profile has been calculated yet.

The second stage of the modeling calculates the temperature profile using Eq. 6-9 with average density and gravity of the upper layer of the mantle obtained for the planet in the first stage. The temperature profile is used to determine the locations of all major known phase transitions in the Earth, from olivine  $(\text{Mg}_{1-x}, \text{Fe}_x)_2\text{SiO}_4$  to a more highly coordinated structure (wadsleyite) that occurs at  $\sim 410$  km depth in the Earth; the transition from a high pressure olivine phase (ringwoodite) to perovskite  $(\text{Mg}_{1-x}, \text{Fe}_x)\text{SiO}_3$  plus ferromagnesiowustite  $(\text{Mg}_{1-x}, \text{Fe}_x)\text{O}$  that occurs at  $\sim 660$  km in the Earth and defines the lower-upper mantle boundary; and the inner-outer core phase transition that corresponds to the depth at which the geotherm intersects the solidus of iron plus an alloy of lighter elements. The solidus for the iron alloy is defined using Lindeman’s law (Poirier 2000b)

$$T_m = T_{m_0} \left( \frac{\rho_0}{\rho} \right)^{2/3} \exp \left\{ \frac{2\gamma_0}{q} \left[ 1 - \left( \frac{\rho_0}{\rho} \right)^q \right] \right\}$$

where  $T_{m_0}$  is the melting temperature at zero pressure.

The thickness of the boundary layers and hence, the temperature profile and phase boundary locations, are calculated iteratively with the gravity and density average values of the upper mantle until convergence is reached and the planet has reached a self-consistent temperature and density profile. This procedure is followed for the ten Super-Earths.

## 3.2 Results

Thermodynamic data varies little for mantle materials but varies widely for core materials. Additionally, there is more uncertainty in the composition of the inner and outer cores. We explore different compositional EOS parameters ( $\rho_0, K_{0,300}, K'_{0,300}, \gamma_0, q, \theta$ ) to test the robustness of the scaling results. Thermodynamic values for the mantle are taken from the compiled and completed data set of Stixrude and Lithgow-Bertollini (2005). Data for the core is less accurate and incomplete. We have chosen to use two extreme end-member compositions to model Earth and Super-Earths of FeO and pure Fe that yield a deficit and an excess in density with respect to PREM of  $200 \text{ kg/m}^3$  and  $300 \text{ kg/m}^3$  respectively. In addition we also use a composition of Fe and 8% by mol Si for the core. All the different cases and thermodynamic values are shown in Table 1.

[Table 1]

In order to address the effects of Fe in the mantle and content of ferromagnesiowustite in the lower mantle we fix the composition of the core to a mixture of Fe and a lighter alloy in the outer and inner core to fit the PREM model more accurately. We compute mixtures of magnesium and iron end members at 0%, 10% and 20% of Fe by mol the mantle; as well as the effect of  $(\text{Mg}_{1-x}, \text{Fe}_x)\text{O}$  by including 10% 30% and 50% by mol in the lower mantle.  $\gamma_0, T_{m_0}$  and  $q$  for the inner core alloy are chosen within reasonable values, such that the melting transition for a one earth-mass planet happens within 30 kms of the inner-outer core boundary in the Earth as described by the PREM model.

There is a wide range of values for the first and second Gruneisen parameters. Large first Gruneisen values yield a hotter interior with steeper solidus. The second Gruneisen parameter controls the curvature of the melting regime. Certain combinations of these parameters, especially with large second Gruneisen values, with a given pressure profile lead to a negative P-T slope in the solidus that is not seen in the pressure regime for the Earth. This was avoided by carefully choosing the values within the uncertainties in the literature, such that the intersection of the thermal profile with the solidus yielded a liquid outer core and a solid inner core. The freedom in these parameters does not affect the values of the scaling laws, mainly because of the smaller effect of temperature. Nevertheless, they do affect structure details such as the exact size of the solid inner core or the presence of a liquid core for planets more massive than the Earth.

These cases exhibit a family of planets with complete solid cores except for Earth. The geotherms we obtained in these cases are closer to the cold geotherm of Brown and Shankland (1981) and are a consequence of the thermodynamic data, in particular the relatively low first Gruneisen parameter and high second Gruneisen parameter (see Fig. 4). The intersection with the solidus happens at a low temperature of  $\sim 3700\text{K}$ , a consequence of a cold geotherm. We test the effects of a warmer geotherm by setting the Gruneisen parameters to large values in the mantle and core (see Table 1 last two rows) to obtain a temperature profile similar to

the one proposed by Stacey (1992c) for the Earth with an inner core boundary temperature of  $\sim 5000\text{K}$ . This yielded all Super-Earths with partially liquid cores. Our last test is to increase the curvature of the solidus (high second Gruneisen parameter) to yield a family of Super-Earths with liquid cores.

[Figure 2]

Figure 2 shows the density and incompressibility profiles of PREM in red and the profiles obtained for the different sets of mineralogical values for one earth-mass. Even though the inner core values for the incompressibility are larger than the ones inferred in PREM, this discrepancy has little effect on the scaling laws. This is clear from the results of the family of planets with no solid inner core that have similar scaling laws.

For planets with masses larger than the Earth, the composition (including heat sources), surface temperature and core mass fraction chosen are equal to those for the one earth-mass case. The heat flow is assumed to scale linearly with mass, as a first attempt to scale internal heat production and secular cooling of more massive planets.

$$4\pi R^2 q_{planet} = Q_{planet} = Q_{earth} \frac{M_{planet}}{M_{earth}} \quad (10)$$

For one composition (10% Fe in mantle minerals and 30%  $(\text{Mg}_{1-x}, \text{Fe}_x)\text{O}$  in the lower mantle), Fig. 3 shows the results for the density profile of the ten Super-Earths. We also include a power law fit of total radius with mass for all the different compositions. Figure 4 shows the corresponding temperature profile, as well as the iron plus a light alloy melting curve for these ten planets. It is clear that the only planet that is hot enough to exhibit an outer liquid core is the Earth. In larger planets the effect of pressure overwhelms the temperature, to yield a solid metal core. Owing to the strong dependence of viscosity in temperature, the internal temperature beneath the top boundary layer is almost independent of mass. Additionally, the thickness of the boundary layer decreases with increasing mass as a consequence of higher Rayleigh numbers for more massive planets

[Figure 3, Figure 4]

We fit total radius, size of the mantle, core radius and average density with mass in a power law relationship  $\propto M^\beta$  for each of the ten mineral compositions. Figure 5 shows the results of the scaling coefficient  $\beta$  for all the sets, Table 1 includes the results as well as the thermodynamic values used in each case. All fits are quite linear in log space except for the average density relationship that has a slight curvature.

A one earth-mass planet with a core composition of FeO yields a density deficit com-

pared to the Earth, as expected (see Fig.2). In this family of planets, the first three exhibit completely liquid cores and the rest have completely solid cores. Figure 5 shows the results from this composition in a grey down-pointed triangle. Due to the lighter composition in the core, given a fixed core mass fraction, more massive planets accommodate more of their mass in their mantle, yielding a larger scaling exponent for the mantle thickness. Due to the  $r^3$  geometric factor this translates into smaller core radius and total radius exponents. In turn, a smaller exponent for the total radius translates into a larger exponent for the average density. Nevertheless, this composition gives extreme values for the scaling of the bulk properties for Earth-like planets and hence may be regarded as an extreme case. An FeSi8% composition yields liquid cores for all the Super-Earths planets. A one earth-mass planet is still too dense to match PREM. A core composition of pure Fe yields a one earth-mass planet with an excess in density with respect to PREM and solid cores for the family of planets.

Circles, stars and plus signs in Fig. 5 correspond to 10%, 30% and 50% ferromagnesiowustite in the lower mantle. Wustite is lighter and more compressible than perovskite. Hence more wustite in the lower mantle decreases the total radius and mantle thickness scaling exponent. However, more wustite changes the scaling of the core radius very little. Consequently the scaling for the average density increases with the content of ferromagnesiowustite in the lower mantle.

[Figure 5]

The values labeled 'hot' in Fig. 5 are the sets in which we chose high thermal parameters. For the geotherm that matches that of Stacey 1992a, the whole family of planets exhibit a liquid outer core. The values shown in green and pink asterisks have the same composition of 10%Fe and 30%  $(\text{Mg}_{1-x}, \text{Fe}_x)\text{O}$  and different geotherms. The scaling for radius of a warmer interior increases with respect to the cold geotherm case, whereas the core radius scaling decreases slightly, producing a larger  $\beta$  for mantle thickness and lower average density. The results shown with a purple asterisk are produced with the same composition and a high second Grüneisen parameter that allows for all Super-Earths to have a completely liquid core except for Earth.

The scaling parameters do not vary much with these hotter geotherms because of the smaller effect of temperature on the density of the planet compared to the pressure effect. Choosing different values for the thickness of the bottom boundary layer would make the core hotter or colder by no more than  $\sim 300\text{K}$ , not enough to yield different scaling laws for the bulk properties of these planets.

The effects included to calculate the pressure are the hydrostatic pressure derived from the 3rd order Birch-Murnaghan equation of state and the thermal pressure derived from the Debye theory. It is known that the contribution from electronic pressure is non-negligible in metals at high pressures but is still smaller than the thermal pressure contribution. Stixrude and Wasserman

(1997) showed that at a pressure of 350 GPa, close to the Earth’s central pressure, the electronic pressure has an 8% contribution. This is the error in pressure that can be expected for Super-Earths. Despite this uncertainty, the scaling can be considered to be robust by looking at the results in Table 1 for the cases of pure FeO and pure Fe in the outer core with a deficit and excess in density (hence in pressure), with respect to PREM, of  $\sim 10\%$  and  $16\%$  respectively. Including this term in the pressure would make the core material more incompressible in very massive planets, making it more difficult to accommodate mass in the core. Thus, the effect would be to yield comparatively smaller radii with large masses, decreasing the scaling exponent slightly. This effect is less important in smaller planets that do not achieve high enough pressures.

## 4 Super-Mercuries

The methodology followed for these planets is identical to that for the Earth-like planets discussed above. We fixed the mineralogy to the best fitting model for the Earth (10% iron end member and 50% ferromagnesiowustite in the lower mantle) and explore different values for core mass fraction and surface temperature to understand their effects in the scaling laws. The masses range between the mass of Mercury and ten mercury-masses.

Figure 6 shows the density and temperature structure for a core mass fraction of 65% and surface temperature of 440K corresponding to Mercury in our solar system (Schubert et al. 1988). The purple star shows data for Mercury. The discrepancy between one mercury-mass and the planet mercury comes mostly from the assumptions on the composition (very close to Earth’s) and the uncertainties in the temperature profile.

With these conditions, no Super-Mercury is hot enough in the core to yield a liquid core and it is clear that high pressure phases in the mantle appear gradually as the mass of the planet increases. Given our assumptions we can not conclude that the planet Mercury in our solar system has a completely solid core.

[Figure 6]

The low central temperatures are a consequence of the relatively small size of the planet. The pressure at the center of the most massive Super-Mercury is  $\sim 260$  GPa. Higher surface temperatures would produce a hotter interior. Figure 7 shows the effect of higher surface temperatures and different core mass fractions. The exponent for the scaling laws does not change considerably except for the case in which the surface temperature is 1500K. Figure 8 shows how in this case, the P-T curves intersect the solidus yielding about half of the Super-Mercuries with a liquid and a solid inner core. Thus, the first four planets lie on a different slope than the next six Super-Mercuries in the core size and average density figures. The cases for a surface temperature of 440K and 2000K exhibit a completely solid core or a completely

liquid core respectively.

[Figure 7, Figure 8]

The power law exponent to the fits of radius, mantle thickness, core size and average density with mass for the different cases of surface temperature and core mass fraction are summarized in Table 2. The relationship  $R \propto M^\beta$  between the total radius and mass for the Super-Mercuries is closer to the expected  $\beta = \frac{1}{3}$  if the average density was constant, than for Super-Earths. We attribute this effect to the smaller size of the Super-Mercuries that limit the compressibility and thermal effects on the properties of the planet.

[Table 2]

## 5 Conclusions

The exercise of scaling Earth to larger masses gives an insight into the internal structure of a massive terrestrial planet. These are planets that due to their large compressional effects and high internal temperatures exhibit a mass to radius relationship that deviates from the cubic power relationship for constant density scaling. For various compositions the relationship is  $R \propto M^{0.267-0.272}$ .

Super-Mercuries, owing to their small size, do not achieve significant pressures and temperatures to largely alter the cubic exponent, having a relationship of  $R \propto M^{\sim 0.3}$  for different core mass fractions and surface temperatures. Space missions are biased to detecting planets with smaller periods, making them closer to its parent star and hence hotter. It has been shown here that there may be cases where the surface temperature may have a noticeable effect on the internal density of the planets.

In general, given a pressure regime, the uncertainties in the thermodynamic data for the mantle and core do not affect the scaling exponents of the bulk properties significantly. The same can be said for the uncertainty in the thickness of the bottom boundary layer and core mass fraction. The pressure regime is mostly controlled by the composition of the planet, therefore different exponents in the scaling laws would be expected for planets composed of rock and ice/water.

It is important to note that the implicit assumption that the Super-Earths and Super-Mercuries have a thermal evolution similar to Earth, such that we can use a scaled parameterized convection may restrict the realm of families for which the scaling laws derived here are valid.

### ACKNOWLEDGEMENTS

We would like to thank Sang-Heon Shim for the valuable help on the topic of equations

of state and Lars Stixrude and Carolina Lithgow-Bertollini for making their thermodynamic data available to us before publication. We are grateful for the useful reviews by Christophe Sotin.

## References

- Anderson, O., Isaak, D. G., 2000. Calculated melting curves for phases of iron. *Am. Mineral.* 85, 376–385.
- Baglin, A., Auvergne, M., Barge, P., Buey, J., Catala, C., Michel, E., Weiss, W., Team, C., 2002. Corot: asteroseismology and planet finding. In: Favata, F., Roxburgh, I. (Eds.), *Proceedings of the First Eddington Workshop*, ESA SP-485, pp. 17–24. Noordwijk.
- Beckwith, S., Sargent, A. I., 1996. Ai circumstellar disks and the search for neighboring planetary systems. *Nature* 383, 139–144.
- Birch, F., 1952. Elasticity and constitution of the earth's interior. *J. Geophys. Res.* 57, 227–286.
- Bodenheimer, P., Pollack, J., 1986. Calculations of the accretion and evolution of giant planets: The effect of solid cores. *Icarus* 67, 391–408.
- Borucki, W. J., Koch, D., Basri, G., Brown, T., Caldwell, D., Devore, E., Dunham, E., Gautier, T., Geary, J., Gilliland, R., A.Gould, Howell, S., Jenkins, J., 2003. Kepler mission: a mission to find earth-size planets in the habitable zone. In: Fridlund, M., Henning, T. (Eds.), *Proceedings of the Conference on Towards Other Earths: DARWIN/TPF and the Search for Extrasolar Terrestrial Planets*, ESA SP-539, pp. 69–81. Noordwijk.
- Brown, J., Shankland, T., 1981. Thermodynamic parameters in the earth as determined from seismic profiles. *Geophys. J. R. Astron. Soc* 66, 576–596.
- Charbonneau, D., Brown, T., Noyes, R., Gilliland, R., 2002. Detection of an extrasolar planet atmosphere. *Astrophys. J.* 568, 377–384.
- Davies, G., 1980. Thermal histories of convective earth models and constraints on radiogenic heat production in the earth. *Journal of Geophysical Research* 85, 2517–2530.
- Dziewonski, A., Anderson, D., 1981. Preliminary reference earth model. *Physics of the Earth and Planetary Interiors* 25, 297–356.
- Fearn, D., 1998. Hydromagnetic flow in planetary cores. *Rep. Prog. Phys* 61, 175–235.
- Hayashi, C., 1981. Structure of the solar nebula, ... *Progr, Theoret. Phys. Supp.* 70, 35–53.
- Ida, S., Lin, D., 2004. Toward a deterministic model of planetary formation. i. a desert in the mass and semimajor axis distributions of extrasolar planets. *Astrophys. J.* 604, 388–413.

- Ikoma, M., Emori, H., Nakazawa, K., 2000. Formation of giant planets: Dependences on core accretion rate and grain opacity. *Astrophys. J.* 537, 1013–1025.
- Konacki, M., Torres, G., Sasselov, D., Jha, S., 2005. A transiting extrasolar giant planet around the star ogle-tr-10. *Astrophys. J.* 624, 372–377.
- Labrosse, S., Poirier, J., Mouel, J. L., 2001. The age of the inner core. *Earth Planet. Sci. Lett.* 190, 111–123.
- Lin, J., Campbell, A. J., Heinz, D. L., 2003. Static compression of iron-silicon alloys: Implications for silicon in the earth’s core. *J. Geophys. Res.* 108. doi:10.1029/2002JB001978.
- Lunine, J., Raymond, S., Quinn, T., 2004. Can habitable terrestrial planets co-exist with hot jupiters? In: abs.P32A-03. AGU.
- Mizuno, H., 1980. Formation of the giant planets. *Prog. Theor. Phys. Supp.* 64, 544–557.
- O’Connell, R. J., Hager, B., 1980. On the thermal state of the earth. In: Dziewonski, A. M., Boschi, E. (Eds.), *Physics of the Earth’s Interior*. North Holland, pp. 270–317.
- Poirier, J., 2000a. Equations of state. In: *Introduction to the Physics of the Earth’s Interior*. Cambridge University Press, pp. 63–109.
- Poirier, J., 2000b. Melting. In: *Introduction to the Physics of the Earth’s Interior*. Cambridge University Press, pp. 110–155.
- Raymond, S., Quinn, T., Lunine, J., 2004. Making other earths: dynamical simulations of terrestrial planet formation and water delivery. *Icarus* 168, 1–17.
- Schubert, G., M.N.Ross, Stevenson, D., Spohn, T., 1988. Mercury’s thermal history and the generation of its magnetic field. In: Vilas, F., Chapman, C., M.S.Matthews (Eds.), *Mercury*. The University of Arizona Press, Tucson, pp. 430–432.
- Stacey, F., 1992a. *Physics of the Earth*. Brookfield Press.
- Stacey, F., 1992b. Reference data. In: *Physics of the Earth*. Brookfield Press, pp. 404–414.
- Stacey, F., 1992c. Reference data. In: *Physics of the Earth*. Brookfield Press, pp. 458–459.
- Stevenson, D., 1982. Formation of the giant planets. *Planet. Space Sci.* 30, 755–764.
- Stixrude, L., Lithgow-Bertollini, C., 2005. Thermodynamics of mantle minerals-i. physical properties. *Geophys. J. Int* 161, INPRESS.
- Stixrude, L., Wasserman, E., 1997. Composition and temperature of earth’s inner core. *J. Geophys. Res.* 102, 24729–24739.
- Turcotte, D., Schubert, G., 2002. *Geodynamics*, Chapter Fluid Mechanics, pp. 226–291. Cambridge University Press.

- Uchida, T., Wang, Y., Rivers, M. L., Sutton, S. R., 2001. Stability field and thermal equation of state of  $\epsilon$ -iron determined by synchrotron x-ray diffraction in a multianvil apparatus. *J. Geophys. Res.* 106, 21779–21810.
- Vidal-Madjar, A., Etangs, A. D., Desert, J., Ballester, G., Ferlet, R., Hebrard, G., Mayo, M., 2003. An extended upper atmosphere around the extrasolar planet hd209458b. *Nature* 422, 124–125.
- Wetherill, G., 1990. Formation of the earth. *Annu. Rev. Earth. Planet. Sci.* 18, 205–256.
- Williams, Q., Knittle, E., 1997. Constraints on core chemistry from the pressure dependence of the bulk modulus. *Physics of the Earth Planetary Interiors* 100, 49–59.
- Wyatt, M. C., Dent, W., J.S.Greaves, 2003. Scuba observations of dust around lindroos stars: evidence for substantial submillimetre disc population. *Mon. Not. Royal Astr. Soc.* 342, 876–888.

**TABLE CAPTIONS** Table 1. Thermodynamic data for the core and the mantle used in calculating the density, pressure and temperature profiles of Earth and the family of SuperEarths. Data for the mantle is taken from (Stixrude and Lithgow-Bertollini 2005) and different compositions were tested for the core including extreme end member cases such as FeO and pure Fe for the outer core. Different ratios of Fe and ( $\text{Mg}_{1-x}, \text{Fe}_x$ ) (Wu) are chosen for the mantle with a fixed composition for the core. For this runs,  $\gamma$  in the inner core has to be chosen with high precision to yield an inner core boundary within 30 Km of the Earth's transition. The last two entries correspond to warm geotherms that have an inner core boundary temperature of  $\sim 5000$  K that can only be achieved with very large Gruneisen parameters. The value of  $\gamma_0 = 2.9$  was chosen for all mantle materials.

Table 2. Scaling law exponent of radius, mantle thickness, core radius and average density as a function of mass for planets with masses ranging from one mercury-mass up to ten times the mass of mercury. The table shows the effect of surface temperature and core mass fraction (CMF) in the scaling laws. Larger CMF yields larger exponents of the scaling of radius, mantle and core size with mass and a smaller exponent of density with mass. The effect of the surface temperature is not monotonic because at  $T_{surf} = 440K$  and  $T_{surf} = 2000K$  all the planets have either completely solid or liquid cores respectively, but at  $T_{surf} = 1500K$  the transition occurs of the first four planets exhibiting a solid core, and the rest a partially liquid core.

Table 2

$T_{\text{surf}}$	CMF	Radius	Mantle	Core	Density
440	65	0.3058	0.3160	0.3023	0.0827
1500	65	0.2991	0.3312	0.2891	0.1027
2000	65	0.3000	0.3247	0.2923	0.1000
440	50	0.3032	0.3072	0.3012	0.0903
440	80	0.3094	0.3371	0.3042	0.0718

Table 1

Mantle		Outer Core	Inner Core	$\beta$			
Fe%	Wu%	$(\rho_0, K_{0,300}, K_{0,300}', \gamma_0, q, \theta)^*$	$(\rho_0, K_{T0}, K_{T0}', \gamma_0, q, \theta)$	R	D	R <sub>cmb</sub>	$\rho$
10%	30%	FeO (6200 <sup>c</sup> , 126 <sup>c</sup> , 4.8 <sup>c</sup> , 2.2 <sup>a</sup> , 1.62 <sup>a</sup> , 421 <sup>a</sup> )	Fe (8171, 135, 6.0, 1.36, 0.91, 998) <sup>b</sup>	0.263	0.316	0.217	0.211
10%	30%	Fe%8wSi (7793, 141, 5.7, 2.2, 1.62, 421) <sup>a</sup>	Fe (8171, 135, 6.0, 1.36, 0.91, 998) <sup>b</sup>	0.272	0.293	0.252	0.186
10%	30%	Fe (8171, 135, 6.0, 1.36, 0.91, 998) <sup>b</sup>	Fe (8171, 135, 6.0, 1.36, 0.91, 998) <sup>b</sup>	0.272	0.286	0.258	0.185
10%	10%	Fe+alloy (6800 <sup>d</sup> , 165 <sup>d</sup> , 4.2 <sup>d</sup> , 1.9 <sup>e</sup> , 1 <sup>e</sup> , 998 <sup>a</sup> )	Fe+alloy (7990 <sup>d</sup> , 200 <sup>d</sup> , 5.2 <sup>d</sup> , 1.734 <sup>d</sup> , 1 <sup>e</sup> , 998 <sup>a</sup> )	0.271	0.298	0.247	0.187
10%	30%	Fe+alloy	Fe+alloy $\gamma = 1.698^d, \theta = 998^a$	0.270	0.296	0.247	0.190
10%	50%	Fe+alloy	Fe+alloy $\gamma = 1.577, \theta = 464^d$	0.269	0.293	0.247	0.195
0%	50%	Fe+alloy	Fe+alloy $\gamma = 1.583^d$	0.269	0.293	0.247	0.194
20%	50%	Fe+alloy	Fe+alloy $\gamma = 1.647^d, \theta = 998^a$	0.268	0.294	0.247	0.195
10%	30%	Fe+alloy $(6800, 136, 4.8, 2.5, 1, 421)$	Fe+alloy $(8051, 217, 4.9, 2.06, 0.91, 464)^d$	0.271	0.300	0.244	0.188
10%	30%	Fe+alloy $\gamma_0 = 2.9, q = 1^d$	Fe+alloy $(8051, 217, 4.9, 2.338, 1.5, 464)^d$	0.271	0.299	0.247	0.186

\*  $\rho$  in kg/m<sup>3</sup>,  $K_{0,300}$  in GPa and  $\theta$  in Kelvin;

<sup>a</sup> Lin et al. 2003;

<sup>b</sup> Uchida et al. 2001;

<sup>c</sup> Williams and Knittle 1997;

<sup>d</sup> assumed in order to fit density and bulk compressibility to PREM;

<sup>e</sup> Anderson and Isaak 2000

## FIGURE CAPTIONS

Figure 1. Schematic temperature profile with conductive gradients through out the boundary layers at the top and bottom of the mantle and adiabatic gradients through out the bulk mantle and core. The bottom boundary layer is chosen to be half the size of the surface boundary layer.

Figure 2. Density (left) and incompressibility (right) of one earth-mass planets with different compositions. The surface of the planet is always to the right of the figures. Solid profiles in blue, green and yellow have 0%, 10% and 20% by mol of Fe end member in the mantle minerals respectively. The dotted line and dashed line have 0% and 30% by mol of ferromagnesiowustite in the lower mantle. The pink and purple solid lines are the high thermal profile runs.

Figure 3. Density profile (left) for one to ten earth-masses. Each planet has 32.59% of its mass in the core and a composition of 10% iron in the mantle and 30% ferromagnesiowustite in the lower mantle. Power law fit (right) of total radius as a function of mass for ten different mineral compositions. The red star shows data for Earth.

Figure 4. Temperature structure (left) and melting regime (right) for Super-Earths with a composition of 10% iron in the mantle and 30% ferromagnesiowustite in the lower mantle. Solid line shows the geotherm proposed by (Brown and Shankland 1981). Solidus for a solid solution of iron and a light element alloy. The Earth is the only planet that intersects the solidus to yield a liquid outer core. All other planets have completely solid cores for this particular set of thermodynamic data.

Figure 5. Power law fit coefficients of total radius (top left), mantle thickness (top right), core radius (bottom left) and average density (bottom right) with mass for Earth-like planets with masses ranging from 1-10 earth-masses. Blue, green and yellow symbols mean a composition of 0%, 10% and 20% of Fe in mantle minerals. Open circles, asterisks and plus symbols mean 0%, 30% and 50% of ferromagnesiowustite with the rest perovskite in the lower mantle. Pink asterisk represents a warm geotherm that allows for all Super-Earths to have a liquid outer core. Purple asterisk has a suitable Lindeman melting law that produces completely molten cores for planets with two to ten earth-masses.

Figure 6. Density (right) and temperature (left) profiles of planets with masses ranging from one to ten mercury-masses with a core mass fraction of 65% and 440K surface temperature.

Figure 7. Scaling laws for Super-Mercuries for total radius (top left), mantle thickness (top right), core size (bottom left) and average density (bottom right). Blue:  $T_{\text{surf}} = 440\text{K}$  % CMF=65%, Green:  $T_{\text{surf}} = 440\text{K}$  % CMF=50%, Black:  $T_{\text{surf}} = 440\text{K}$  % CMF=80%, Yellow:

$T_{\text{surf}} = 1500\text{K}$  %  $\text{CMF}=65\%$ , Red:  $T_{\text{surf}} = 2000\text{K}$  %  $\text{CMF}=65\%$ . Purple stars show the data for the planet Mercury in our solar system.

Figure 8. Melting regime for Super-Mercuries with a 65% core mass fraction. Three family of planets are shown: with surface temperature of 2000K that exceeds the solidus, thus all planets have completely liquid cores; a second family with surface temperature of 1500K that intersects the solidus yielding 4 planets with liquid cores and 6 with solid inner cores; the last family with a surface temperature of 440K that exhibits completely frozen cores.

FIGURES Figure 1

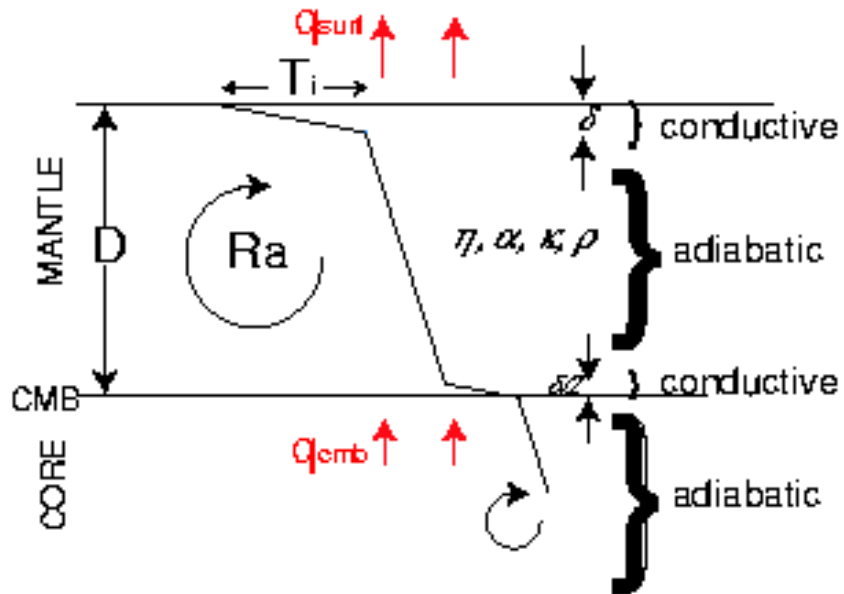


Figure 2

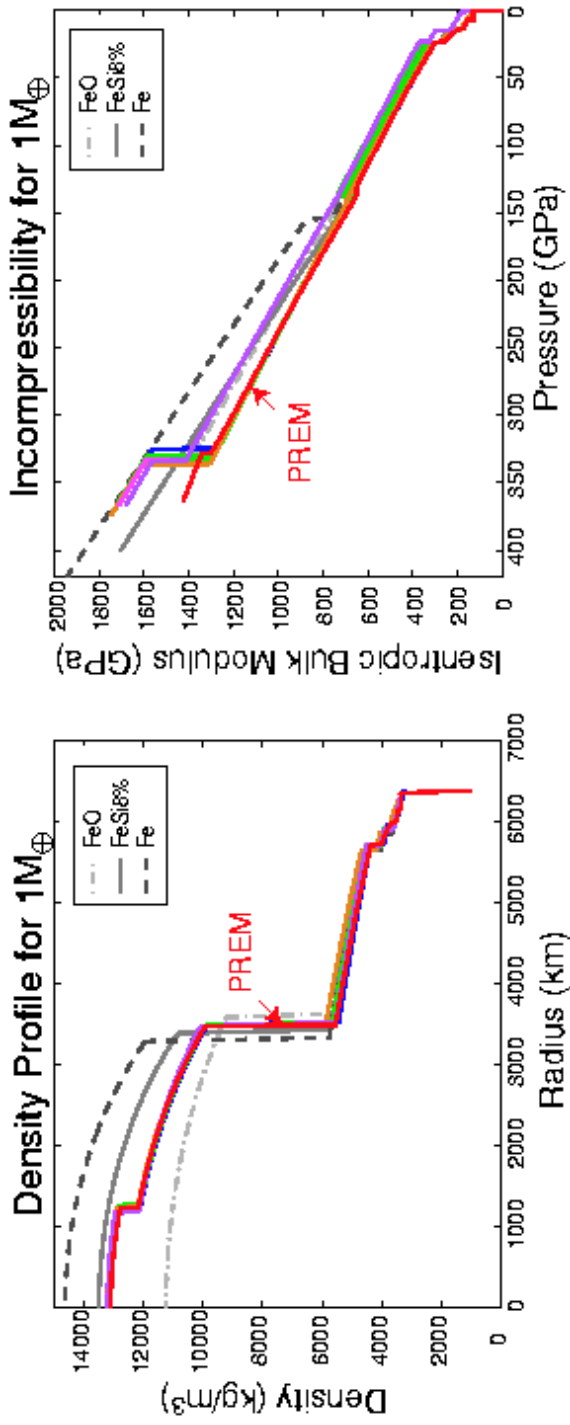


Figure 3

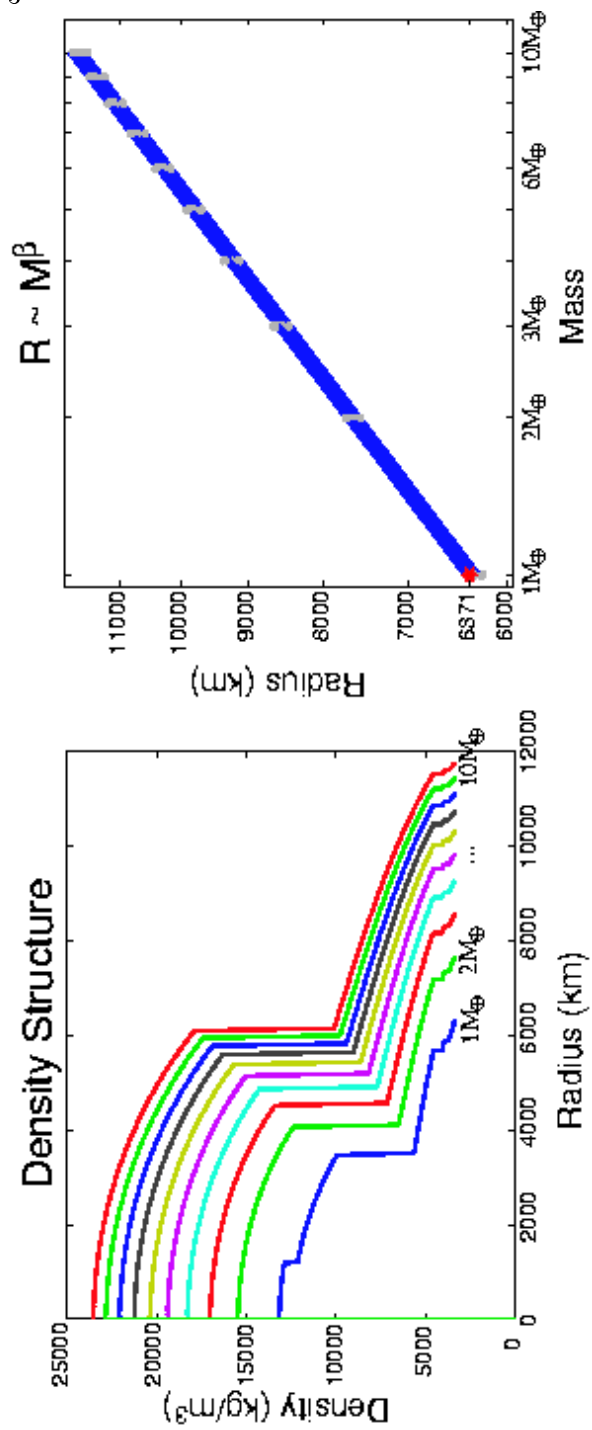


Figure 4

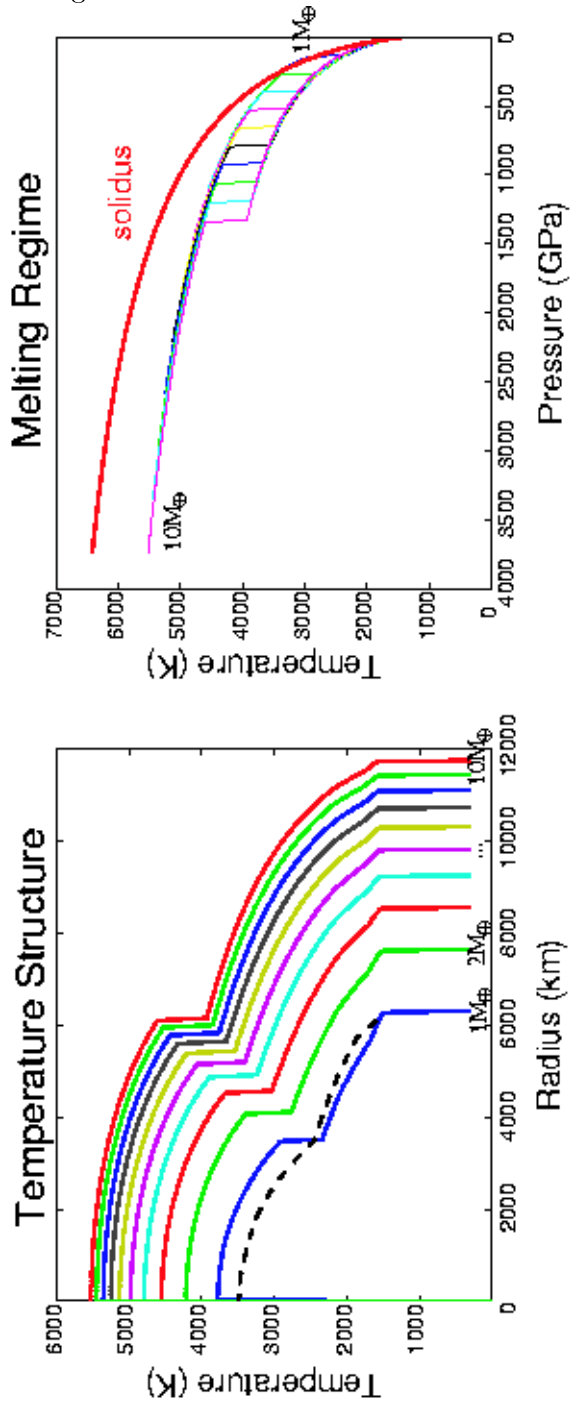


Figure 5

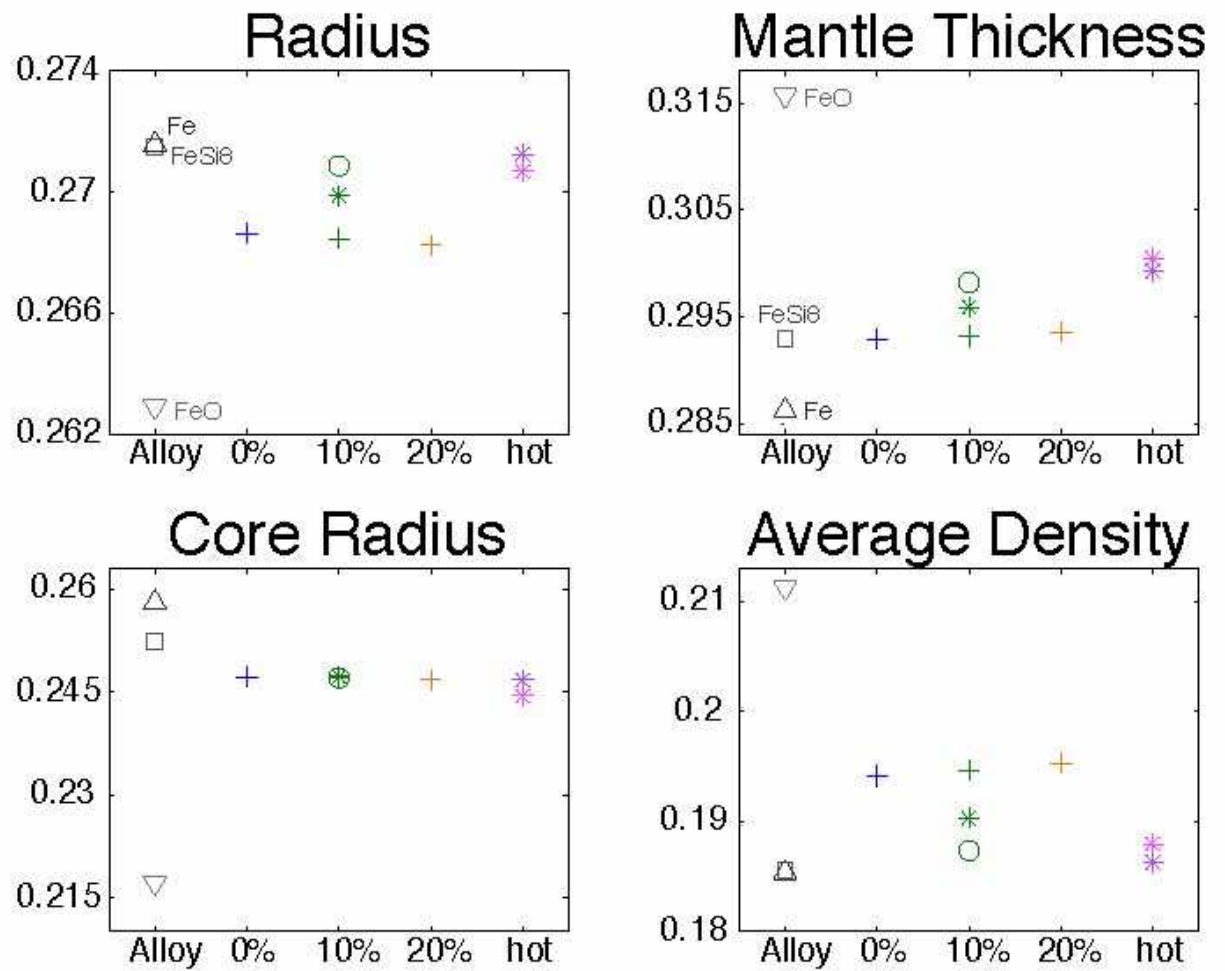


Figure 6

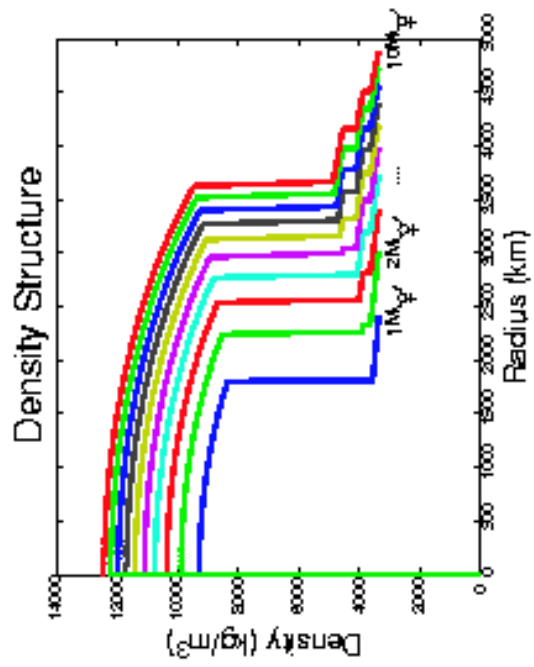
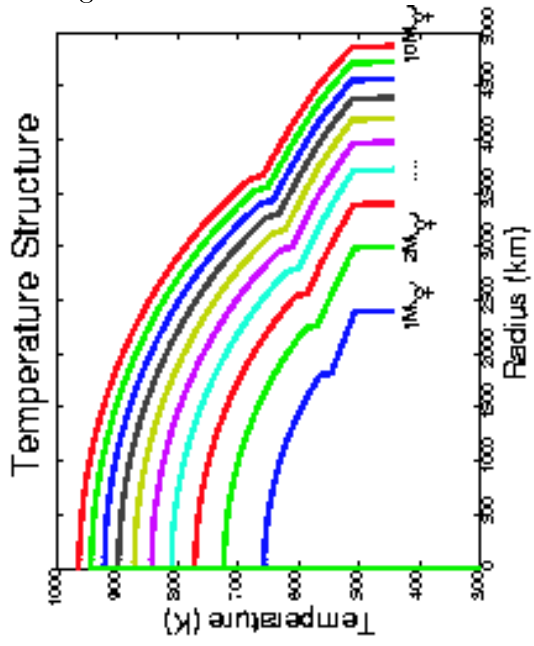


Figure 7

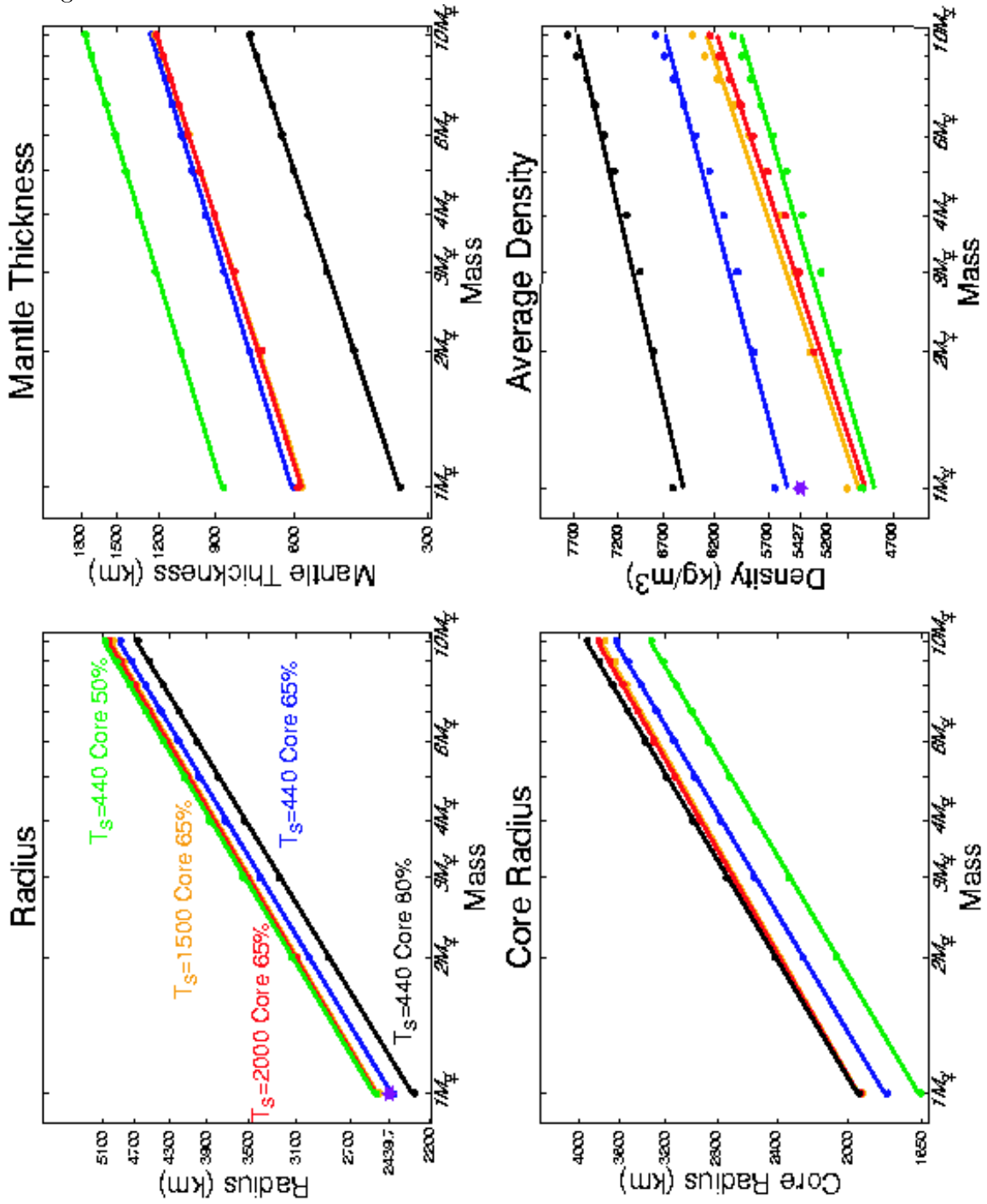


Figure 8

